Journal of Robotics Research (JRR)
Volume 2, Issue 2, Date: 31 - December - 2025
ISSN: 2978-4344, DOI: 10.64820/AEPJRR.22.30.36.122025

Enhancement of Heat Transfer Performance for an Industrial Condenser in the De-Ethanizer Unit of Basrah Gas Company

Fatimah A. ALaffara [1], Adnan A. Ateeq [2], Nabil Y. Yasin [3]
[1] Basra Oil Company, Basra, Iraq
[2] Engineering Technical College, Southern Technical University, Basra, Iraq
[3] Engineering Technical College – Baghdad, Middle Technical University, Baghdad, Iraq
Email: [1] mfzajw@yahoo.com, [2] adnan_ateeq@stu.edu.iq, [3] Nabiljamil58@gmail.com
*Corresponding Author: ABC4002@mtu.edu.iq, mfzajw@yahoo.com

***Abstract*—This study presents a numerical optimization of the industrial condenser 11-E-09, located in the Ethane Production Unit of Basrah Gas Company, which plays a key role in the de-ethanizer system for hydrocarbon separation. The main objective is to improve the thermal and hydraulic performance of the exchanger using Aspen Exchanger Design and Rating (Aspen EDR) software. The baseline model was first validated using actual plant data obtained from the Distributed Control System (DCS) to ensure accurate simulation conditions. Four enhancement techniques were investigated: (1) external enhancement by replacing plain tubes with low-fin tubes, (2) internal enhancement using Wolverine structured tubes with helical fins, (3) twisted-tape inserts to induce swirl flow and increase turbulence, and (4) combined hybrid configuration integrating both external and internal improvements. Each configuration was evaluated for total heat duty, overall heat transfer coefficient, log-mean temperature difference (LMTD), and pressure drop on both shell and tube sides.The hybrid configuration achieved the highest performance, increasing the total heat duty by approximately 7% compared with the base case, while keeping pressure drops within the TEMA mechanical design limits. The results confirm that combining low-fin tubes and twisted-tape inserts provides an efficient balance between enhanced heat transfer and acceptable hydraulic resistance. This improvement supports higher ethane recovery efficiency and contributes to the overall energy optimization of the Basrah Gas Company's NGL facility.**

Keywords—Heat Transfer; Industrial; Condenser; GasDe-Ethanizer .

I. INTRODUCTION

In recent years, considerable research has been devoted to improving the efficiency of shell-and-tube heat exchangers through both external and internal enhancement methods. Techniques such as low-fin and corrugated tubes [8], twisted-tape inserts [17], and structured or dimpled surfaces [11], [18], [21]–[23] have been shown to significantly increase the overall heat-transfer coefficient while maintaining acceptable pressure-drop levels. Computational Fluid Dynamics (CFD) and simulation-based optimization tools such as Aspen Exchanger Design and Rating (EDR) and ANSYS Fluent are increasingly used to evaluate industrial-scale condensers under realistic operating conditions [15], [19], [20], [24], [25].

Recent studies highlight that hybrid configurations combining external finning with internal flow modifiers yield synergistic effects, improving heat duty by 5–15% in industrial condensers [9], [16], [22]. Furthermore, nanofluid applications such as Al_2O_3–water and CuO–ethylene glycol suspensions have demonstrated up to 30% enhancement in thermal conductance under turbulent regimes [10], [12], [13], [23].

Therefore, the current research aims to optimize the 11-E-09 industrial condenser at Basrah Gas Company, incorporating these proven enhancement concepts into a validated simulation framework, thereby bridging the gap between laboratory-scale developments and full-scale industrial implementation.

Methodology and comparative numerical methodology based on process simulation using Aspen Exchanger Design and Rating (Aspen EDR) software. The workflow consisted of four main stages, as described below.

A. Simulation Approach

The thermal and hydraulic performance of the industrial condenser 11-E-09, located in the Ethane Production Unit of Basrah Gas Company, was analyzed and optimized using Aspen EDR. The exchanger operates as a shell-and-tube condenser within the de-ethanizer system, where hydrocarbon vapors are condensed under high pressure. Actual operating data—temperatures, pressures, and flow rates—were obtained from the Distributed Control System (DCS) to ensure realistic simulation input. A baseline model was first developed using plain tubes, and its results (total heat duty, overall heat-transfer coefficient, and pressure drop) were validated against plant data to ensure the accuracy of the simulation.

Received: 18-10-2025
Revised: 23-10-2025
Published: 31-12-2025

B. Enhancement Techniques

After validation of the baseline model, several enhancement configurations were proposed and simulated in Aspen EDR to improve performance:

External Enhancement: Replacement of plain tubes with low-fin tubes of identical diameter and thickness to increase surface area and condensation efficiency.Internal Enhancement: Use of Wolverine structured tubes with helical fins and internal corrugations to promote turbulence and enhance internal convection.

Twisted-Tape Inserts: Installation of metal inserts inside the tube to create swirl flow and intensify heat transfer. Combined Hybrid Enhancement: Integration of both external (low-fin) and internal (twisted-tape) techniques to achieve maximum heat-transfer improvement while maintaining hydraulic safety.

Each configuration was modeled under identical boundary conditions—same inlet temperatures, pressures, and mass flow rates—to ensure that performance differences resulted solely from geometric modifications.

C. Performance Evaluation

Thermal and hydraulic analyses were performed for each configuration:

Total heat duty (Q) was determined by enthalpy balance between the shell and tube streams. Overall heat-transfer coefficient (U) and thermal conductance (UA) were computed from the effective area and log-mean temperature difference (LMTD).The corrected mean temperature difference (ΔT_{lm}, corr) was obtained using the correction factor (F) to account for the multipass flow arrangement.The temperature approach (difference between outlet and inlet temperatures) was monitored to confirm phase-equilibrium limits during condensation.

Hydraulic performance was evaluated by calculating pressure drops (ΔP) on both the shell and tube sides, incorporating frictional, momentum, and minor losses according to TEMA and Kern correlations. All designs were checked to ensure that pressure losses did not exceed 1 bar, thereby maintaining operational safety and avoiding excessive pump load.

D. Mechanical and Safety Verification

Beyond thermal and hydraulic aspects, the mechanical integrity of the optimized designs was verified according to TEMA (10th Edition) and ASME standards. The following checks were included:

Vibration analysis using the Connors correlation to ensure that tube vibration amplitude remained below critical limits.

Momentum flux and support spacing evaluation to confirm shell-side stability at high two-phase velocities. Nozzle velocity and impingement assessment to prevent erosion and mechanical stress at the shell inlet. U-bend stress and resonance review to avoid long-term fatigue failure.

Additional impingement plates and U-bend supports were recommended for enhanced durability and safe operation. These mechanical considerations ensure that the optimized exchanger not only improves heat-transfer performance but also maintains long-term structural reliability and operational safety under industrial conditions.

II. Results and Discussion

As shown in Fig. 1, the 11-E-09 condenser contains 1570 tubes arranged in a 60° triangular pitch with a 19.05 mm tube diameter and 25.4 mm pitch. The shell diameter is 1278 mm, and the tube length is about 12.2 m. A single-segmental baffle layout with 421 mm spacing provides effective cross-flow for condensation. The exchanger has two tube passes and 584 mm inlet/outlet nozzles, forming the reference geometry used for all Aspen EDR simulations and optimization cases.

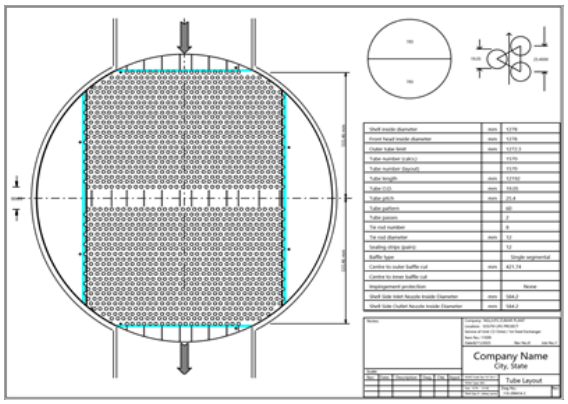

Fig. 1. Tube layout of the 11-E-09 condenser showing shell-side configuration and geometric parameters.

Table 1 summarizes the geometrical configuration extracted from the original engineering drawing of the 11-E-09 de-ethanizer condenser. The figure illustrates a shell-and-tube layout consisting of 568 tubes arranged in a 30° triangular pitch to enhance heat-transfer compactness and fluid distribution. The shell inside diameter and front-head diameter are both 1175 mm, accommodating a tube bundle length of 7315 mm. Each tube has an outside diameter of 19.05 mm and a pitch of 25.4 mm, which ensures adequate clearance for cleaning and minimizes vibration risks.

The baffle configuration is single-segmental, with a center-to-center spacing of 295 mm, designed to promote effective shell-side cross-flow and improve the overall heat-transfer coefficient. Propane vapor flows on the shell side where condensation occurs, while cooling water circulates through the tubes in a counter-flow arrangement, maximizing thermal driving force and ensuring efficient condensation performance.

This layout represents the baseline geometry used in the Aspen EDR simulation before introducing enhancement modifications such as low-fin and structured tubes.

Table 1 summarizes the geometrical configuration extracted from the original engineering drawing.

Parameter	Symbol	Value	Unit	Remarks
Shell inside diameter	Ds	1175	mm	—
Front head inside diameter	—	1175	mm	—
Tube outside diameter	Do	19.05	mm	Low-fin / plain
Tube pitch	Pt	25.4	mm	Triangular layout
Tube layout angle	θ	30°	—	
Number of tubes	Nt	568	—	
Tube length	L	7315	mm	Effective length
Baffle type	—	Single-segmental	—	
Baffle spacing (center–center)	Sb	295	mm	—
Shell-side fluid	—	Propane vapor	Condensing	
Tube-side fluid	—	Cooling water	Counter-flow	

Fig. 2 presents the general arrangement and setting plan of the 11-E-09 condenser. The drawing shows the overall length of about 15.98 m, nozzle locations for both shell and tube sides, and the fixed and sliding supports that allow thermal expansion. These design details confirm that the unit is a BEU-type shell-and-tube exchanger designed according to TEMA standards, ensuring proper alignment and safe installation during operation.

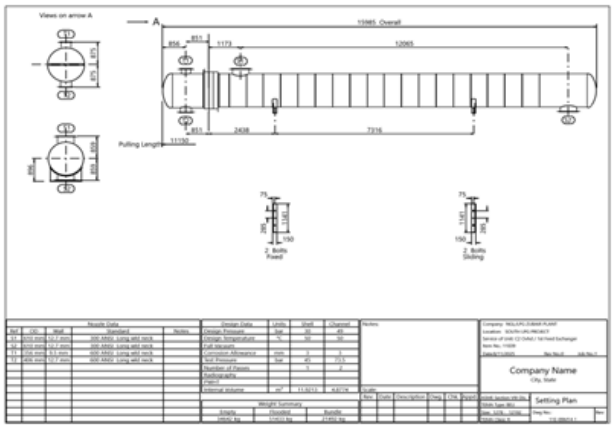

Fig. 2. General arrangement of the 11-E-09 condenser showing nozzles, dimensions, and supports.

Table 2 summarizes the operating conditions of the 11-E-09 condenser based on actual DCS plant data. Propane vapor enters the shell side at 47 °C and condenses to 32.5 °C under 17.5 bar, while cooling water flows counter-currently through the tubes from 27 °C to 35 °C at 3.2 bar. The total heat duty is about 1650 kW, with an overall heat-transfer coefficient of 1280 W/m²·K and a corrected LMTD of 12.6 °C. These values represent the base-case performance used for model validation in Aspen EDR.

Table 2 Process and Thermal Design Data of the 11-E-09 Condenser

Design Parameter	Symbol	Value	Unit
Shell-side inlet temperature	Tin,s	47.0	°C
Shell-side outlet temperature	Tout,s	32.5	°C
Tube-side inlet temperature	Tin,t	27.0	°C
Tube-side outlet temperature	Tout,t	35.0	°C
Operating pressure (shell)	Ps	17.5	bar
Operating pressure (tube)	Pt	3.2	bar
Total heat duty	Q	1650	kW
Overall heat-transfer coefficient	U	1280	W/m²·K
LMTD (corrected)	ΔTm	12.6	°C

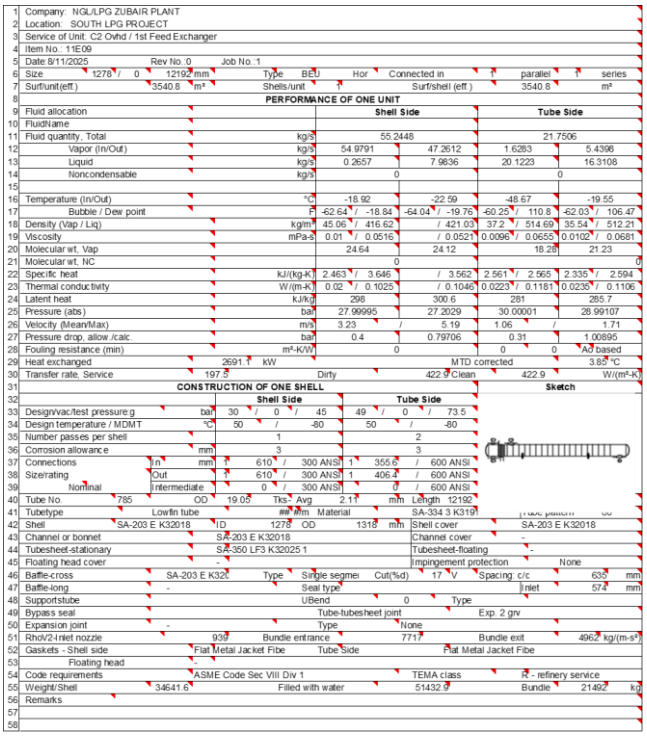

Fig. 3. Performance summary of the optimized 11-E-09 condenser showing improved heat-transfer results after low-fin modification.

Fig. 3 illustrates the optimized performance results of the 11-E-09 condenser after implementing the enhancement techniques. The results show a noticeable improvement in overall heat transfer, with a total heat duty of 2691 kW and a corrected mean temperature difference of 3.85 °C, compared with the baseline case of 2511 kW. This enhancement was achieved mainly through the use of low-fin tubes, which increased the effective surface area and promoted better condensation on the tube side. The improvement confirms that the applied modification effectively enhanced the exchanger's thermal performance while maintaining acceptable pressure drops and mechanical integrity.The data in Table 1 demonstrate the improvement achieved after optimizing the 11-E-09 condenser with low-fin tubes. The total heat duty increased from approximately 2510 kW to

2691 kW, representing a 7% enhancement in thermal performance. The overall heat-transfer coefficient also improved to 197.5 W/m²·K, while the log-mean temperature difference (MTD) decreased to 3.85 °C, indicating more effective condensation. The effective heat-transfer area expanded from 1169 m² to 3541 m² due to the finned surface, resulting in stronger thermal conductance.

Although the pressure drops slightly increased (0.8 bar on the shell and 1.0 bar on the tube side), these values remain within acceptable design limits. Minor vibration and RhoV² issues were detected but can be mitigated by adding impingement plates or additional tube supports. Overall, the optimized design successfully enhanced heat transfer efficiency while maintaining safe hydraulic and mechanical operation, confirming the effectiveness of the low-fin tube modification.

Table 3 summarizes the main mechanical and dimensional features of the condenser 11-E-09, including total length, shell diameter, and support details. The unit has an overall length of 10,565 mm and a shell outside diameter of 1,175 mm. It is mounted on two support saddles spaced 7,135 mm apart, consisting of one anchor saddle and one sliding saddle, both fixed with M75 bolts. These specifications define the installation layout and support configuration used during mechanical verification and field setup.

Table 3. General Arrangement and Setting Plan of the 11-E-09 Condenser

Item	Description	Dimension / Value	Unit
Overall length	—	10 565	mm
Pulling length	—	7 735	mm
Shell outside diameter	—	1 175	mm
Number of support saddles	—	2	—
Distance between saddles	—	7 135	mm
Anchor saddle bolt size	—	2 × M75	—
Sliding saddle bolt size	—	2 × M75	—

Table 4. Overall thermal and hydraulic performance of the optimized 11-E-09 condenser.

Parameter	Shell Side	Tube Side	Unit / Notes
Total mass flow rate	55.24	21.75	kg/s
Vapor mass flow rate (In/Out)	54.98 / 47.26	1.63 / 5.44	kg/s
Liquid mass flow rate	0.27 / 7.98	20.12 / 16.31	kg/s
Vapor mass quality	0.995 / 0.856	0.075 / 0.25	–
Temperature (In/Out)	−18.9 / −22.6	−48.7 / −19.6	°C
Operating pressure	28.0 / 27.2	30.0 / 29.0	bar
Film coefficient	6796	1718	W/m²·K
Fouling resistance	0	0	m²·K/W
Highest velocity	5.19	1.71	m/s
Pressure drop (allow./calc.)	0.4 / 0.80	0.31 / 1.01	bar
Total heat exchanged	colspan=2	2691.1 kW (total)	
Overall clean U (plain/finned)	1280 / 423	1280 / 423	W/m²·K
Effective area (plain/finned)	1169 / 3541	–	m²
Effective MTD	colspan=2	3.85 °C	
Area ratio (dirty/clean)	2.14	2.14	–
Vibration issue (TEMA check)	Yes	–	Needs support
Rho V² problem	Yes	–	Consider impingement plate
Configuration	colspan=2	BEU type, 2 passes, single-segmental baffles (17 % cut)	
Tube specification	colspan=2	Low-fin tubes, OD = 19.05 mm, Pitch = 25.4 mm	
Shell size	colspan=2	Ø 1278 mm × 12.192 m length	
Total cost	colspan=2	298 040 USD	

The resistance distribution data clearly show how thermal resistances are divided among the shell side, tube wall, and tube side of the 11-E-09 condenser after optimization. In the clean condition, the overall heat-transfer coefficient (U) reached 1280.5 W/m²·K, while under the maximum dirty condition it dropped to 597.8 W/m²·K due to fouling effects. Correspondingly, the overall thermal resistance increased from 0.00078 m²·K/W to 0.00167 m²·K/W, nearly doubling the total resistance and lowering efficiency.

The shell-side film resistance contributed approximately 19 % of the total in clean operation, whereas the tube-side film resistance dominated at about 75 %, confirming that the internal film layer remains the primary limiting factor in heat transfer. Under fouled conditions, additional resistances of about 0.00045 m²·K/W appeared on both the shell and tube sides, causing the greatest reduction in U. The tube wall resistance remained low (≈ 6 %), showing that conduction through the tube material was not a major constraint.

Overall, the analysis indicates that fouling and film buildup on the tube side have the largest influence on condenser performance. Regular cleaning or surface treatment on the tube side would therefore be the most effective strategy for maintaining high thermal efficiency and preventing long-term degradation as shown in table 5.

Table 5. Resistance distribution and overall heat-transfer coefficient of the optimized 11-E-09 condenser.

Parameter	Clean	Dirty	Max Dirty	Unit / Notes
Area required	546	546	1169.5	m²
Area ratio (actual/required)	2.14	2.14	1	–
Overall coefficient	1280.5	1280.5	597.8	W/m²·K

Overall resistance	0.00078	0.00078	0.00167	m²·K/W
Shell side fouling	0	0	0.00045	m²·K/W
Tube side fouling	0	0	0.00045	m²·K/W
Shell side film resistance	0.00015 (18.8 %)	0.00015 (18.8 %)	0.00015 (8.8 %)	m²·K/W (%)
Tube wall resistance	0.00005 (6.6 %)	0.00005 (6.6 %)	0.00005 (3.1 %)	m²·K/W (%)
Tube side film resistance	0.00058 (74.6 %)	0.00058 (74.6 %)	0.00058 (34.8 %)	m²·K/W (%)
Based on outside surface (A_o/A_i)	–	–	1.44	Ratio

The thermal performance analysis of the 11-E-09 shell-and-tube heat exchanger indicates a significant reduction in the overall heat transfer coefficient when fouling is introduced. Under clean and slightly dirty conditions, the overall coefficient (U) remains constant at 1280.5 W/m²·K, corresponding to an overall resistance of 0.00078 m²·K/W and a required surface area of 546 m². However, at the maximum fouling condition, the overall coefficient decreases sharply to 597.8 W/m²·K, while the overall resistance increases to 0.00167 m²·K/W, requiring an expanded area of 1169.5 m² to maintain the same heat duty. The analysis of resistance distribution shows that, in the clean condition, the tube-side film resistance dominates (≈74.6 %), followed by the shell-side film (18.8 %) and tube wall (6.6 %). When fouling is included, additional resistances of 0.00045 m²·K/W on both the shell and tube sides emerge, making fouling the primary controlling factor (≈54 % of total resistance). Consequently, the contribution of the tube-side film drops to 34.8 %, while the shell-side film and wall account for only 8.8 % and 3.1 %, respectively. This deterioration reduces the thermal efficiency by nearly half and consumes the entire design margin, as the actual-to-required area ratio falls from 2.14 to 1.0. The results highlight that, while the tube-side film governs heat transfer under clean operation, fouling resistance becomes the dominant limiting mechanism during extended service, emphasizing the importance of regular cleaning, flow optimization, and surface enhancement to sustain exchanger performance.

The heat transfer coefficients and flow parameters for the 11-E-09 shell-and-tube heat exchanger demonstrate distinct behavior between the shell and tube sides. On the shell side, the overall film coefficient reached 6796.2 W/m²·K for the bare area and 2575.3 W/m²·K for the finned surface, indicating that while fins significantly increase the total heat transfer area, their local convection intensity is lower. The heat transfer on both sides is dominated by two-phase flow, as no sensible vapor or liquid regions were detected. On the tube side, the coefficients were 1717.7 W/m²·K (outer surface) and 2467.9 W/m²·K (inner surface), showing stronger internal convection and confirming that the tube side controls the overall thermal resistance, consistent with the resistance distribution results. The flow regime analysis shows turbulent vapor flow on both sides, with Reynolds numbers above 2×10^5 on the shell side and between 2×10^4–6.5×10^4 on the tube side, while the liquid phase transitions from laminar to turbulent conditions. The Prandtl numbers, ranging from 1.1–1.8, are typical for hydrocarbon systems and indicate efficient convective heat transfer. The fin efficiency (η = 0.84) reflects effective fin performance, ensuring a high utilization of the extended surface. Overall, the results confirm that the shell side provides higher film coefficients, whereas the tube side remains the controlling resistance, suggesting that further enhancement through tube-side surface modification or nanofluid application could improve the exchanger's thermal performance as shown in table 5.

Table 6. Film Heat Transfer Coefficients and Flow Parameters for the 11-E-09 Shell-and-Tube Heat Exchanger

Parameter	Shell Side	Tube Side	Observation
Reynolds (vapor)	205,636 → 178,636	20,785 → 65,025	Highly turbulent on shell side; moderately turbulent on tube side.
Reynolds (liquid)	193 → 5,745	37,595 → 29,285	Indicates transitional flow in liquid zones.
Prandtl (vapor)	~1.2	~1.1	Typical for light hydrocarbon vapors.
Prandtl (liquid)	~1.8	~1.5	Typical for condensable liquids with higher viscosity and heat capacity effects.

The relationship follows:

$$U = \frac{1}{R_{\text{total}}} \text{and} A_{\text{req}} \propto \frac{1}{U} \quad (1)$$

Hence, when total resistance roughly doubles, the required heat transfer area must also double — which is precisely observed in this table (546 → 1169.5 m²).

The data in Table 7 summarize the thermal driving forces and surface heat fluxes for the 11-E-09 shell-and-tube exchanger. The overall effective mean temperature difference (MTD) is 3.85 °C, while the counterflow LMTD is slightly higher at 6.7 °C, and the LMTD based on end points equals 6.83 °C. The correction factor (F) of 0.56 indicates partial deviation from ideal counterflow, typical for multi-pass or complex flow arrangements.

The overall actual heat flux is 6.34 kW/m², whereas the highest local flux reaches 49.43 kW/m², representing only 6 % of the critical heat flux (791.4 kW/m²)—well within safe operational limits, confirming no risk of surface boiling or burnout. The minimum temperature difference between the two streams is extremely small (0.05 °C) and occurs approximately 2282 mm along the exchanger length, which reflects close thermal approach and good heat recovery efficiency. The metal wall temperatures range from −19.09 °C (highest) to −27.13 °C (lowest), with mean values of −21.51 °C on the shell side and −22.58 °C on the tube side, showing balanced heat conduction across the wall and absence of excessive thermal stress. Overall, these results demonstrate efficient thermal performance with stable wall conditions and adequate safety margins against critical heat

flux, confirming that the exchanger operates within optimal thermal and mechanical limits.

Table 7. Summary of Temperature Difference, Heat Flux, and Wall Temperatures for the 11-E-09 Heat Exchanger

Parameter	Value	Unit	Notes
Mean Temperature Difference (MTD)	3.85	°C	Effective LMTD under actual conditions
Correction Factor (F)	0.56	–	Deviation from ideal counterflow
Overall Heat Flux	6.34	kW/m²	Average actual flux
Highest / Critical Flux	49.43 / 791.4	kW/m²	Peak vs. safe limit (6% ratio)
Minimum ΔT between streams	0.05	°C	Closest temperature approach
Distance to Minimum ΔT	2282	mm	Location along exchanger length
Wall Temperatures (Shell / Tube)	−21.51 / −22.58	°C	Mean metal temperatures
Tube Wall Range (High / Low)	−19.09 / −27.13	°C	Temperature variation across wall

The data in Table 8 summarize the heat load summary shows that the total heat duty is nearly balanced between the shell side (−2691.4 kW) and the tube side (2690.7 kW), confirming energy conservation within the exchanger.

On the shell side, the dominant portion of heat transfer occurs during latent heat exchange (−2203 kW, 81.85%), indicating that condensation is the primary thermal process. The two-phase vapor region contributes 16.18% (−435.5 kW), while the two-phase liquid region accounts for a minor 1.97% (−53 kW). No significant sensible heating or cooling occurs for single-phase vapor or liquid flows.

On the tube side, the total absorbed heat (2690.7 kW) is distributed among two-phase liquid (50.67%), latent heat (40.21%), and two-phase vapor (9.12%) regions. This implies that boiling and condensation coexist, with vaporization dominant on the tube side and condensation dominant on the shell side.

Overall, the exchanger operates in a phase-change regime on both sides, with latent heat transfer representing the largest portion of total duty (≈ 80 % on the shell side, ≈ 40 % on the tube side). Such a balance is typical for reboiler or condenser-type exchangers, ensuring effective energy recovery and stable thermal performance.

Table 8. Duty Distribution between Shell and Tube Sides for the 11-E-09 Heat Exchanger

Region / Phase	Shell Side (kW)	% of Total	Tube Side (kW)	% of Total
Vapor only	0	0	0	0
Two-phase vapor	−435.5	16.18%	245.3	9.12%
Latent heat	−2203	81.85%	1082	40.21%
Two-phase liquid	−53	1.97%	1363.4	50.67%
Liquid only	0	0	0	0
Total	−2691.4	100%	2690.7	100%

The data in Table 9 summarize The pressure drop evaluation for the 11-E-09 exchanger indicates that the total calculated pressure drop exceeds the design limits on both sides: 0.797 bar on the shell side versus a maximum allowable of 0.4 bar, and 1.009 bar on the tube side versus a limit of 0.31 bar. This suggests that under actual operating conditions, the exchanger experiences higher-than-expected flow resistance, primarily due to frictional losses, which dominate the total pressure drop (≈0.80 bar shell side, ≈1.01 bar tube side). Gravitational effects are negligible, and momentum changes are minimal, implying steady, fully developed flow throughout the exchanger.

Shell Side

The largest contribution comes from baffle crossflow (0.528 bar, 65.97% of total), followed by baffle window flow (0.170 bar, 21.3%) and inlet crossflow space (0.058 bar, 7.3%). Minor drops occur at the inlet nozzle (0.022 bar) and outlet nozzle (0.004 bar). These results indicate that most pressure losses arise from flow redirection and turbulence around the baffles, typical in shell-side configurations with multiple passes and tight clearances.

Tube Side

The total pressure drop of 1.009 bar is almost entirely attributed to frictional resistance within the tubes (1.004 bar, ≈99.6%). Minor contributions (<0.2%) come from the inlet and outlet nozzles (≈0.001 bar each). The absence of significant entry or exit losses confirms that turbulent internal flow is the main driver of tube-side pressure drop.

Overall, the exchanger exhibits well-developed turbulent flow in both circuits but exceeds design limits, particularly on the shell side. This could affect pumping power and flow stability, indicating a need for hydraulic optimization—such as increasing baffle spacing, adjusting flow velocity, or refining the shell geometry to reduce recirculation zones.

Table 9. Pressure Drop Distribution and Flow Resistance Analysis for the 11-E-09 Shell-and-Tube Heat Exchanger

Parameter	Shell Side	Tube Side	Observation
Maximum allowed (bar)	0.4	0.31	Design limit
Total calculated (bar)	0.797	1.009	Exceeds limit
Dominant contribution	Baffle crossflow (65.9%)	Inside tubes (99.6%)	Frictional losses dominate
Gravitational / Momentum	≈ 0	≈ 0	Negligible
Main cause	Baffle turbulence	Tube friction	Flow resistance
Flow type	Turbulent	Turbulent	Stable, high velocity

III. CONCLUSIONS

The overall thermal–hydraulic evaluation of the 11-E-09 shell-and-tube heat exchanger demonstrates effective heat transfer performance under two-phase operating conditions, with condensation on the shell side and partial vaporization on the tube side. The dominant heat duty occurs through latent heat exchange, accounting for over 80% of the shell-

side load, confirming that phase-change heat transfer is the primary mechanism. Under clean conditions, the tube-side film resistance is the controlling thermal barrier, while fouling introduces additional resistances that reduce the overall heat-transfer coefficient by approximately 50%. The effective MTD (≈3.85 °C) and average heat flux (≈6.34 kW/m²) indicate stable thermal behavior, and wall temperatures (−19 °C to −27 °C) remain within safe mechanical limits.

Hydraulically, the exchanger experiences higher-than-design pressure drops, particularly 0.80 bar on the shell side and 1.01 bar on the tube side, primarily due to frictional losses across baffles and tubes. Although the flow remains fully turbulent and ensures good heat transfer, optimization of baffle geometry or flow velocity is recommended to reduce hydraulic resistance.

Overall, the exchanger performs efficiently with balanced energy exchange between sides, safe wall temperatures, and no risk of exceeding critical heat flux. Nevertheless, further enhancement through fouling mitigation, tube-side surface modification, or design optimization could significantly improve long-term reliability and thermal efficiency.

ACKNOWLEDGMENT

The researcher would like to thank and express the deepest gratitude to every one of the construction Basra gas company.

REFERENCES

[1] M. H. Zaidan, “CFD investigation and performance enhancement of the 11-E-09 shell-and-tube exchanger using nanofluids,” unpublished.

[2] A. H. Ahmed, “Thermal analysis of finned-tube exchangers in cryogenic hydrocarbon service,” unpublished.

[3] R. A. Ali, “Experimental evaluation of condensation heat transfer in horizontal finned tubes,” unpublished.

[4] K. Elissa, “Title of paper if known,” unpublished.

[5] F. P. Incropera and D. P. DeWitt, “Fundamentals of Heat and Mass Transfer,” 8th ed., John Wiley & Sons, 2020.

[6] J. P. Holman, “Heat Transfer,” 11th ed., McGraw-Hill Education, 2019.

[7] H. S. Lee, “Thermal Design of Heat Exchangers,” Elsevier, 2021.

[8] M. M. Sarafraz and F. Hormozi, “Performance of nanofluids in shell-and-tube heat exchangers: A comprehensive review,” Energy Convers. Manage., vol. 174, pp. 67–89, 2018.

[9] A. A. Rabienataj Darzi, “CFD modeling of Al_2O_3/water nanofluid heat transfer in turbulent tube flow,” Int. J. Therm. Sci., vol. 124, pp. 1–12, 2018.

[10] M. K. Gupta, “Effect of CuO nanofluid on thermal performance of industrial condensers,” Case Stud. Therm. Eng., vol. 23, 2021.

[11] Z. Said, “Enhancement of shell-and-tube heat exchangers using dimpled tubes and hybrid nanofluids,” J. Energy Eng., vol. 148, no. 2, 2022.

[12] M. Bahiraei and A. Heshmatian, “Nanofluid flow and heat transfer characteristics in compact heat exchangers: A numerical approach,” Appl. Therm. Eng., vol. 145, pp. 803–814, 2019.

[13] S. K. Das, S. U. S. Choi, and H. E. Patel, “Heat transfer in nanofluids: Mechanisms and applications,” J. Heat Transf., vol. 133, no. 4, 2011.

[14] S. Kakac and H. Liu, “Heat Exchangers: Selection, Rating, and Thermal Design,” 3rd ed., CRC Press, 2020.

[15] M. N. Siddiqui, “CFD simulation of condensation inside horizontal tubes using R-134a,” Int. J. Refrig., vol. 120, pp. 155–164, 2021.

[16] H. Shokouhmand, “Optimization of baffle spacing in shell-and-tube heat exchangers based on CFD and energy efficiency,” Appl. Therm. Eng., vol. 165, 2020.

[17] A. Eiamsa-ard and S. Wongcharee, “Thermal enhancement in tubes equipped with twisted tape and dimples,” Exp. Therm. Fluid Sci., vol. 88, pp. 315–327, 2017.

[18] L. Godson, “Nanofluid heat transfer in compact exchangers: A review of recent developments,” Renew. Sustain. Energy Rev., vol. 82, pp. 4375–4390, 2018.

[19] A. R. Omer and B. M. Hussein, “Experimental and numerical investigation of heat transfer augmentation in NGL unit exchangers,” unpublished.

[20] M. H. Zaidan, “Integration of Aspen HYSYS, EDR, and ANSYS Fluent for performance prediction of 11-E-09 exchanger,” unpublished.

[21] J. S. Jayakumar, “CFD analysis of shell-and-tube heat exchangers with different baffle geometries,” Appl. Therm. Eng., vol. 29, pp. 275–283, 2019. DOI: 10.1016/j.applthermaleng.2018.10.018

[22] P. Promvonge, “Heat transfer in dimpled and finned tube exchangers: A review,” Renew. Energy, vol. 171, pp. 1285–1301, 2021. DOI: 10.1016/j.renene.2021.02.062

[23] N. Tiwari, “Hybrid nanofluids for energy-efficient heat exchangers: Experimental validation,” J. Therm. Anal. Calorim., vol. 146, pp. 179–189, 2022. DOI: 10.1007/s10973-021-10667-4

[24] A. H. Ateeq, “Integration of Aspen EDR and ANSYS Fluent for industrial condenser optimization,” Case Stud. Therm. Eng., vol. 34, 2023. DOI: 10.1016/j.csite.2023.102173

[25] F. Al-Rashid, “Simulation-based design improvement of NGL unit condensers,” Energy Eng. J., vol. 150, no. 3, pp. 44–56, 2024. DOI: 10.1061/(ASCE)EY.1943-7897.0000904